IPP-Report

IPP Max-Planck-Institut für Plasmaphysik

P. Franzen, O. Vollmer, A. Stäbler

Spectroscopic Determination of the Species Distributions of the ASDEX Upgrade Neutral Beam Injection Systems

IPP 4/278
December 1998

Spectroscopic Determination of the Species Distributions of the ASDEX Upgrade Neutral Beam Injection Systems

P. Franzen, O. Vollmer, A. Stäbler

Max-Planck-Institut für Plasmaphysik

Abstract

The neutral beam injection system of ASDEX Upgrade consists of two almost identical beam lines with four sources each. The main difference is the ion source: conventional arc sources are used for the first beam line, whereas the second beam line is equipped with new RF sources. Both types of sources deliver a mixture of atomic and molecular ions of hydrogen and deuterium. Hence the injected neutral beam consists not only of full energy neutral atoms, but also of atoms with half and third energy. The distribution of the different hydrogenic particles (protons and molecular ions) in the extracted beam, the species distribution, and the distribution of the neutral hydrogen atoms with the different energies in the injected neutral beam, the power distribution, of both beam lines have been measured by H_α Doppler shift spectroscopy in the neutralizers as well as in the duct between the injection box and the ASDEX Upgrade torus vessel for hydrogen and deuterium beams.

The RF sources yield a higher proton fraction than the arc sources. Accordingly, a higher fraction of full energy atoms is injected into the plasma: in the case of 60 kV deuterium operation, this amounts to about 72% of the total injected power for the RF sources, compared to about 65% for the arc sources. The agreement between the power distributions derived from the duct and the neutralizer measurements is satisfactory; the fact that the full energy fraction revealed from the duct measurements is slightly higher especially at higher energies may be related to the simplifying assumption of an infinitely thick neutralizer target in the calculations.

Contents

List of Figures

List of Tables

1 Introduction

The injection of neutral hydrogen or deuterium atoms with energies in the several keV range is the primary heating method for today's fusion experiments (for a general overview see e.g. Ref. [1]). The energetic neutral atoms are created by extracting positive ions from suitable ion sources, accelerating the ions to the high energies, and finally neutralizing the energetic ions by collisions with a gas target in the so-called neutralizer.

However, not only protons or deuterons are created in the ion source, but also the hydrogen or deuterium molecular ions H_2^+ and H_3^+ or D_2^+ and D_3^+, respectively. These molecular ions are also extracted and accelerated, and are dissociated in the neutralizer. Hence, the final neutral beam consists not only of neutral atoms with the full acceleration energy, but also of neutral atoms with half and third energy. In systems with a high oxygen content in the plasma or a (small) leak in the water-cooled acceleration grids, also water molecular ions (H_2O^+ or HDO^+ and D_2O^+, respectively) are created and accelerated, leading to neutral hydrogen or deuterium atoms with energies of 1/18, 1/19, 2/19 and 1/10 of the extraction energy, respectively.

In order to assess the effect of neutral beams on a plasma, e.g. the energy deposition profile in the plasma or the total fuelling, the power distribution of the different species is an important parameter, i.e. what fraction of the total input power is carried with full, half and third energy. On the other hand, the different types of ion sources can also be characterized by the species distribution, i.e. the distribution of the different ions in the extracted ion beam.

The species and power distributions can be determined by means of H_α Doppler shift spectroscopy [2, 3]. During the neutralizing process, excited atoms are created by collisions of the beam species with the background gas. The H_α light, emitted by the atoms with the three different energies, is Doppler shifted and, hence, well separated. The ratio of the intensities of the three Doppler peaks reflects the species distribution in the ion source. From the species distribution, the power distribution can be calculated knowing the neutralization probability of each beam species.

After passing through the magnet, with reflects the non-neutralized ions, the neutral atoms are injected into the plasma through the duct between the beam lines and the torus vessel. Under special conditions — injection in the torus without plasma and magnetic field —, the (much lower) H_α light emission due to collisions of the beam atoms with the residual gas in the duct can also be measured. The intensity of these Doppler peaks is also a measure for the power distribution in the duct and hence in the plasma.

A comparison of the power distributions obtained from the 'extrapolation' of the species distribution in the ion source with that directly measured in the duct gives the possibility to check the assumptions in the models of the physical processes leading to the light emission in the neutralizer: the power distributions obtained from the two measurements should be the same if the models, the assumptions within these models, and the input parameters — such as cross sections — are correct.

2 Neutral Beam Injection Systems at ASDEX Upgrade

The neutral beam injection system of ASDEX Upgrade [4] consists of two almost identical beam lines. Each beam line is equipped with four ion sources of the JET PINI type [5]. Each source is routinely operated at 55 kV for hydrogen (H^0) and 60 kV for deuterium (D^0), respectively. (For the next eperimental period of ASDEX Upgrade starting in Jan. 1999, the sources of the second beamline are upgraded for operation at 70 kV for hydrogen and 100 kV for deuterium, respectively.) A total power of 14 MW H^0 and 20 MW D^0 can be injected in the ASDEX Upgrade torus [6]. Two beams of each beam line are more radial (with radii of tangency of 0.53 m), the remaining two beams of each beam line are more tangential (with radii of tangency of 0.93 m). For comparison, the major plasma radius is 1.65 m, the minor 0.5 m.

The main difference of the two beam lines is the way the ions are created in the ion source: the first beam line is equipped with conventional arc sources [5], where the plasma is created by electrons emitted from hot filaments, whereas the second beam line uses new RF sources [7, 8]. Here the plasma is created by coupling radio frequency power to the electrons ($f \approx 1$ MHz). The latter system is much simpler concerning electrical feedthroughs (only two to the RF coil instead of 48 to the filaments in the arc source) and maintenance.

Each ion source is equipped with a neutralizer box. Hence we will denote in the following the arc sources with the respective neutralizers by SE1 to SE4 (south east beamline), while the RF sources and the attached neutralizers are denoted by NW1 to NW4 (north west beamline).

3 H_α Doppler Shift Spectroscopy

The extracted ion beam from the plasma sources consists of H^+, H_2^+, and H_3^+ ions — and of the respective ions in the case of deuterium beams. All these particles interact with the neutralizer gas leading to neutralization and, for the molecular ions, to dissociation as well as to excitation of the resulting neutral atoms. The spectroscopic analysis of the light emitted by the beam reveals the species distribution in the ion source and the power distribution of the neutral beam in the torus.

A suitable transition with light emitted in the visible spectrum is the hydrogen Balmer α line. The Balmer α light at 656.21 nm (H_α) and 656.10 nm (D_α), respectively, origins from the (n=3)→(n=2) transitions 3s→2p, 3p→2s, and 3d→2p of neutral H or D atoms. The cross section for H_α emission is given by

$$\sigma(H_\alpha) = \sigma_{3s} + \frac{A_{3p-2s}}{A_{3p-2s} + A_{3p-1s}}\sigma_{3p} + \sigma_{3d}, \quad (1)$$

the σ's being the excitation cross sections for the respective fine structure levels and the A's the probability of the respective transition. This equation is only valid if the single fine structure levels are not disturbed by external electrical and magnetic fields. However, as already discussed by Bilau-Faust et al. [9] for the ASDEX beamlines, the magnetic and electric fields, above which Zeemann or Stark effects have to be taken into account, are much higher than the respective fields in the

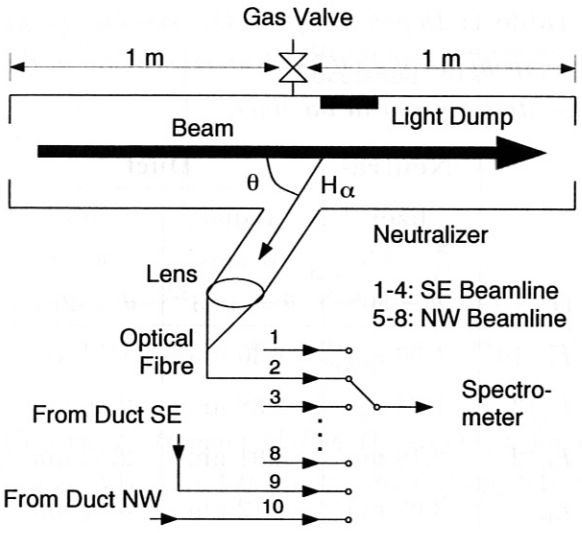

Figure 1: *Principle arrangement of the experimental setup, shown for the neutralizer. The H_α emission can be detected at total 10 measurement points in both beam lines (4 neutralizers and the duct for each beam line); however, only one measurement can be performed at one time. The viewing angle θ is 50° in the neutralizers, and 38.3° and 46.7° in the duct for the radial and the tangential beams, respectively.*

ASDEX Upgrade beamlines.

The H(n=3) level can be populated by charge exchange and collisions between the ions and neutrals in the beam and the gas molecules in the neutralizer or in the duct. A detailed description with the evaluation of the different cross sections can be found in Refs. [9–11]. Beam-beam interactions can be neglected due to the small cross sections and the high gas densities.

In the following, we will describe the experimental setup of our spectroscopic systems, and the calculation of the species and power distributions of the ASDEX Upgrade neutral injection beam lines. These calculations include the integration of the Doppler shifted peaks of the different components, and the different cross sections of the processes leading to the light emission in the neutralizer and in the duct.

3.1 Experimental Setup

The experimental setup is the same as the setup of the H_α measurements of the ASDEX neutral injection beam lines, as described by Bilau-Faust [9]. In fact, most of the components have been transferred to the new systems. The principle arrangement is shown in Figure 1.

The H_α light emitted either in the neutralizers connected with the different ions sources or in the ducts of both beamlines is collected by a Canon camera objective lens (f/D = 1:2/135 mm) and focussed on a 0.6 mm diameter quartz fibre which guides the light into a Czerny-Turner spectrometer with a focal length of 0.5 m (f/6.3) and a grating with 2400 lines per mm. The viewing angle θ is 50° in the neutralizers, and 38.3° and 46.7° in the duct for the radial and the tangential beams, respectively. With this geometry, the H_α emission of the fast neutrals in the beam is red-shifted. The spectrum is monitored by a single line camera with 1024 Si photodiodes. The dispersion was calibrated with gauge lamps (8.7×10^{-3} nm/channel). The wavelength calibration is done by means of the unshifted H_α peak (see below). The integration time of the camera is fixed at 2 seconds.

In order to reduce the background signal and to avoid distortions of the peak shape due to the reflection of light from the metal walls of the neutralizers, as it was observed in the ASDEX [9], W7-AS [12] or in the TFTR [13]

beam lines, specially designed light dumps [14], made out of carbonized aluminum, have been installed in the neutralizers in the direct line-of-sight of the fibre.

The neutralizer spectra are measured in the middle of the neutralizers of each source, at the same position of the gas valves (see Figure 1). Due to the viewing geometry, these spectra are average spectra over the vertical length of the beam; however, H_α light only from the center part of the beam in horizontal direction is detected. The viewing geometry in the duct is rotated by 90°; hence, the spectrometer averages over the horizontal dimension of the beam, but collects light only from the center part in vertical direction.

The duct spectra can only be measured under special conditions: the beams are injected into the 'empty' torus, i.e. no plasma (and no magnetic field) is present. Otherwise, the large light emission from the plasma into the duct outshines the (relatively) small Doppler shifted peaks. Injection into the empty torus means, however, that the total beam power is dumped onto the inner limiter of the torus without any attenuation by the plasma, leading to a sharp temperature rise of the wall areas hitted by the neutral beams. These areas are only inertially cooled. In order to avoid damage, the injection time is limited to a few 100 milliseconds.

3.2 Doppler Shift

The Doppler shift $\triangle\lambda$ of a spectral line at λ_0 emitted by a particle with velocity v is given by (in non-relativistic approximation):

$$\triangle\lambda = -\lambda_0 \frac{v}{c} \cos\theta, \qquad (2)$$

c being the light speed and θ the viewing angle. For deuterium beams with energies of 60 kV, the Doppler shifts of the three energy components are given in Table 1.

Table 1: *Doppler shifts of the possible energy components of a 60 kV deuterium beam in the neutralizer and in the duct.*

	Neutralizer	**Duct**	
		radial beams	tang. beams
D^0	$\theta = 50°$	$\theta = 38.3°$	$\theta = 46.7°$
$E_0/10$	1.06 nm	1.30 nm	1.14 nm
$E_0/3$	1.78 nm	2.38 nm	2.06 nm
$E_0/2$	2.18 nm	2.91 nm	2.52 nm
E_0	3.08 nm	4.12 nm	3.57 nm

The Doppler shifted lines are not monochromatic, but broadened due to various effects, like beam focussing or ion drifts in the source perpendicular to the beam extraction direction. These effects lead to (small) energy deviations and angular distributions in the extracted ion beam.

Figure 2 shows typical spectra, obtained in the neutralizer of source NW3 and in the duct of the NW beam line for a 60 kV deuterium beam. Due to the different energies of the beam species — and the oblique viewing angle, the main D_α peak and the three Doppler shifted peaks of neutral atoms at full, half and third energy in the spectrum are well separated. Hence, the intensity of the H_α light emission of a certain species is proportional to the peak integral of the respective part of the spectrum. The peaks are nearly Gaussian shaped (see Section 3.4), with small deviations at the blue side of the peaks.

Some of the background H_2 molecules are also dissociated leading to thermal neutral excited atoms causing the unshifted H_α peak

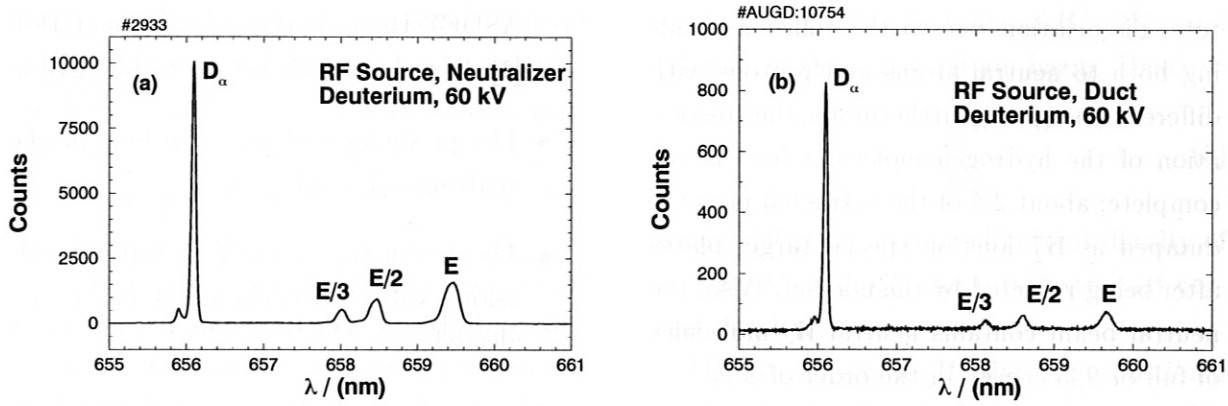

Figure 2: *Doppler shifted D_α spectrum for a 60 kV deuterium beam in the (a) neutralizer of source NW 3 and (b) in the duct of the NW beam line of ASDEX Upgrade.*

in the spectra. The small background also present in the spectrum is mainly due to the dark current of the photodiodes. A clear background reduction can be seen due to the light dumps (see above) in comparison to spectra obtained in the neutralizers of other injection systems [9, 12, 13]. The neutralizer spectrum shows also, that the plasma in the RF ion sources (and also in the arc sources, not shown here) is very clean; there is no indication of any notable oxygen or water impurities as can be seen by the absence of a $E_0/10$ peak at about 657.2 nm (see Table 1).

The signals of the duct spectra are much lower than that of the neutralizer spectra. This is due to the much lower H_2 background pressure in the duct and due to the short beam pulses in combination with the fixed integration time of the camera. This leads also to an increased signal to noise ratio in the duct spectra.

3.3 Calculation of Species and Power Distribution

The calculation of the species and power distributions from the measured H_α spectra consists of two stages: (1) integrating the Doppler shifted peaks of the three energy components; and (2) the integral ratios are converted to the species ratios by means of excitation and neutralizing cross sections. The processes in the neutralizer and in the duct leading to H_α light emission are quite different: in the neutralizer excited neutral atoms are created by collisions of the extracted H^+, H_2^+, and H_3^+ ions as well as already neutralized atoms and molecules with the hydrogen background gas at relatively high pressures (some 10^{-3} mbar); in the duct, however, the remaining neutral H atoms in the beam are excited by collisions with a low pressure H_2 gas (some 10^{-5} mbar). Hence, we will separate our discussion for the two viewing regions.

3.3.1 Neutralizer Measurements

Neutral excited H or D atoms can be created in the neutralizer by charge exchange collisions of the extracted ions as well as by collisions of already neutralized atoms with the background gas. The situation is rather complicated due to the presence of the extracted molecular ions, which undergo partial and/or

total dissociation due to the collisions leading both to neutral atoms and protons with different energies. Furthermore, the dissociation of the hydrogen molecular ions is not complete; about 2% of the extracted power is dumped as H_2^+ ions on special target plates after being reflected by the magnet. Also, the neutral beam contains neutral H_2 molecules of full or 2/3 energy in the order of 1%.

The measured H_α light originates from neutral atoms that de-excite in the viewing region. However, these excited neutral atoms have been created somewhat upstream in the beamline due to the fast movement. With a average lifetime of the hydrogen 3s state of 158 ns, the mean path length of a neutral excited D atom with $E_0/m = 30$ keV/nucleon is about 54 cm.

For simplicity and due to the limited knowledge of the pressure profile between the ion source and the viewing region, we make following assumptions in the discussions below:

- No significant pressure gradient exist between the excitation region and the field of view.
- The excitation region is far enough from the ion source and the target thickness (see below) inbetween is large enough, so that the species composition has reached equilibrium at the excitation region. Hence, the species distribution does not change between the region where the excited atoms are created and the viewing region.
- The current density profile is constant throughout the whole beam. Measurements of the density profiles of the ASDEX Upgrade type of sources at JET [6] showed that this is true within ±10%.
- The production of negative ions in the neutralizer is neglected.
- The destruction of excited states by collisions with the background gas is neglected.

The reactions of the extracted ions with the neutralizing gas lead to the formation of eleven positive ions and neutrals with different energies: protons and neutral hydrogen atoms with full, half and third energy

$$H^+(E_0), H^+(E_0/2), H^+(E_0/3),$$

$$H^0(E_0), H^0(E_0/2), H^0(E_0/3),$$

and the molecules and molecular ions

$$H_2^+(E_0), H_2^+(2E_0/3), H_2^0(E_0),$$

$$H_2^0(2E_0/3), H_3^+(E_0).$$

The $H_2^{0,+}$ particles with the energy of $2E_0/3$ are fragments of the dissociation of the H_3^+ ion. All these particles react with the neutralizer gas via

$$H_i^{0,+}(E_0) + H_2 \rightarrow iH^{0*}(E_0, E_0/2, E_0/3) + \cdots$$

Here and also in the following, E_0 denotes the extraction energy ($E_0 = eU_{ex}$, U_{ex} being the acceleration voltage), whereas E is the energy per nucleon ($E = E_0/m$, m being the mass of the atom in amu). i ranges from 1 to 3 and denotes — also in the following equations — the different beam species.

The rate of creation of excited H atoms in the ($n = 3$) state from one of the above reactions is

$$\frac{dn^*}{dt} = \sigma_k \, v_k \, n_k \, n, \qquad (3)$$

where n^* is the density of excited neutral atoms, σ_k the cross section of the reaction considered, v_k the velocity of the ions or neutrals involved, n_k the density of the fast neutral or charged hydrogen particles, and n the background H_2 density.

In steady state the rate of creation is equal to the rate of decay. Hence, the H_α intensity I_k originating from the considered reaction k is given by

$$I_k = B\ \sigma_k\ v_k\ n_k\ n, \tag{4}$$

B being a constant.

The total H_α intensity showing up in a peak at E_0/i in the measured spectrum is then given by the sum of all appropriate reactions. For example, the H_α intensity I_{E_0} coming from excited neutral atoms with the energy E_0, can be expressed as

$$I_{E_0} = B\ \left(\langle\sigma_+ v_1\rangle\ n^+_{E_0} + \langle\sigma_0 v_1\rangle\ n^0_{E_0}\right) n, \tag{5}$$

where $n^+_{E_0}$ and $n^0_{E_0}$ are the densities of the protons and the neutral hydrogen atoms with energy E_0 in the neutralizer, respectively, and v_1 is the velocity of a particle with an energy of $E_0/1$ (protons and neutral hydrogen atoms). σ_+ and σ_0 are the excitation cross section by charge exchange and by collisions, respectively. They depend on the energy of the ions and neutrals. Similar, but much more complex equations — due to the dissociation of the extracted molecular ions — hold for the H_α intensities at half and third energy, $I_{E_0/2}$ and $I_{E_0/3}$, respectively.

Species Distribution in the Extracted Ion Beam

The different types of ion sources can also be characterized by the species distribution s, i.e. the relative amounts of H^+, H_2^+, and H_3^+ ions in the extracted ion beam. Hence,

$$s_i = \frac{j_i^{\text{ext}}}{j_{\text{tot}}^{\text{ext}}}, \tag{6}$$

where j_i^{ext} is the extracted current density of species H_i^+ and $j_{\text{tot}}^{\text{ext}}$ the total extracted current density.

The intensity of an H_α line is proportional to the density of excited neutral atoms with the energy corresponding to the shift of the peak. This density is again proportional to the density of the neutral and charged particles colliding with the background gas. In order to connect the species distribution to the peak integral ratios, the densities of the neutral atoms and ions in Eq. (5) — and of the molecules and molecule ions in the respective equations for the intensities of the half and third energy components — in the exciting region have to be known. There are several models [10, 11] describing the evolution of the different species due to dissociation and charge exchange processes in dependence on the path length in the neutralizer and the gas density. As result, a function $f_{E_0/i}$ is derived, which connects the measured H_α intensity $I_{E_0/i}$, corresponding to neutral atoms with energy E_0/i, with the species in the ion source:

$$I_{E_0/i} = f_{E_0/i}(\langle nL\rangle)\ j_i^{\text{ext}} \tag{7}$$

This function f depends on the so-called target thickness $\langle nL\rangle$, given by

$$\langle nL\rangle = \int_0^L n\, dl, \tag{8}$$

L being the neutralizer length. The only parameter that depends on $\langle nL\rangle$ and contributes to $f_{E_0/i}(\langle nL\rangle)$ is the neutral beam

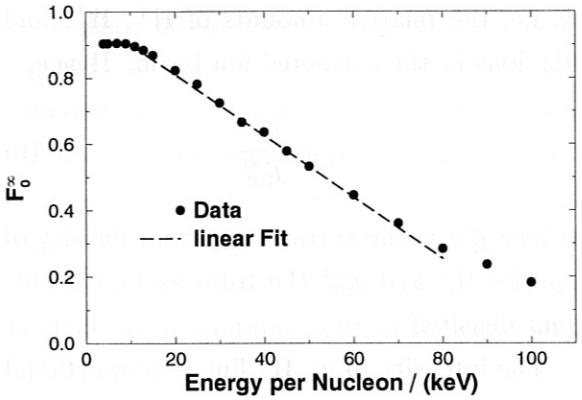

Figure 3: *Equilibrium neutral beam fraction F_0^∞ vs. energy per nucleon for an infinitely thick neutralizer gas target [15].*

fraction F_0 after passing the neutralizer gas target, given by

$$F_0(\langle nL\rangle) = F_0^\infty \left(1 - \mathrm{e}^{-\langle nL\rangle(\sigma_{10}+\sigma_{01})}\right), \quad (9)$$

where F_0^∞ is the asymptotic neutralizing fraction for an infinitely thick neutralizer gas target:

$$F_0^\infty = \frac{\sigma_{10}}{\sigma_{10}+\sigma_{01}}. \quad (10)$$

σ_{10} is the cross section for the neutralizing process

$$\mathrm{H}^+ + \mathrm{H}_2 \rightarrow \mathrm{H}^0 + \ldots,$$

whereas σ_{01} is the cross section for the reverse process, the ionisation

$$\mathrm{H}^0 + \mathrm{H}_2 \rightarrow \mathrm{H}^+ + \ldots$$

.

Figure 3 shows the neutral beam fraction F_0^∞, calculated according to Eq. (10) with the cross sections σ_{10} and σ_{01} from Ref. [15]. F_0^∞ decreases from about 90% at energies $\leq$10 keV per nucleon to about 25% at 80 keV per nucleon. In this energy range, F_0^∞ is nearly linear and can be approximated by

$$F_0^\infty = 0.994 - 9.3\times10^{-3}\,E[\mathrm{keV}], \quad 10\ \mathrm{keV} \leq E \leq 80\ \mathrm{keV} \quad (11)$$

E being the energy per nucleon.

In order to obtain the relative species ratios in the ion source, the function $f_{E_0/i}$ is normalized with respect to the full energy component; this leads to the so-called correction factors C_i:

$$C_1 = \frac{f_{E_0}}{f_{E_0}} = 1, \quad (12a)$$

$$C_2 = \frac{f_{E_0}}{f_{E_0/2}}, \quad (12b)$$

$$C_3 = \frac{f_{E_0}}{f_{E_0/3}}. \quad (12c)$$

The species distribution s_i is then given by

$$s_i = \frac{C_i\, I_{E_0/i}}{\sum_{k=1}^{3} C_k\, I_{E_0/k}}, \quad i = 1..3. \quad (13)$$

Figure 4 shows the corrections factors C_2 and C_3 [16] used in the calculations for a target thickness of 2×10^{20} m^{-2}. The factors are nearly constant over a wide range of $\langle nL\rangle$ down to about 5×10^{19} m^{-2}. Hence, above this target thickness, the target can be considered as infinitely thick. Due to the location of the viewing region in the middle of the neutralizer, the target thickness in the ASDEX Upgrade neutralizers in this and in the excitation region is not well known. However, the total target thickness is large enough so that changes in the gas flow into the neutralizer do not affect the neutral beam fraction. For this, a total target thickness of some 10^{20} m^{-2} is necessary — beam heating effects of the background gas leading to an reduced effective target thickness [17] included.

With the location of the gas valve also in the middle of the neutralizer (see Figure 1), we can assume a nearly constant gas density

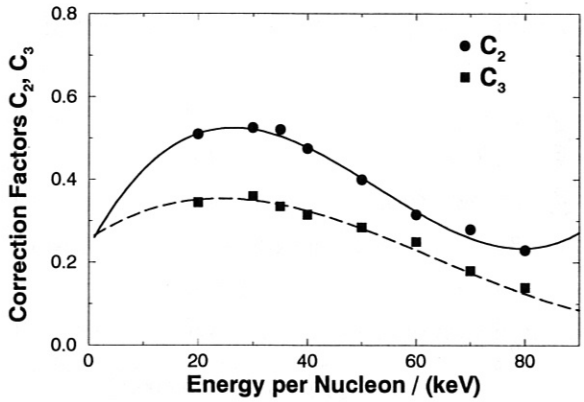

Figure 4: *Corrections factors C_2 and C_3 vs. energy per nucleon for a target thickness of 2×10^{20} m^{-2} (infinitely thick target). The lines are fits to the calculated values [16].*

between the ion source and the viewing region (if we neglect any interchange of gas between source and neutralizer) and a decreasing pressure towards the magnet. Hence, the target thickness at the viewing region may be about three quarters of the total target density. With this and the observations above, the assumption of an 'infinitely thick target' in the calculations above is rather justified. Hence, the species and power distributions derived from the neutralizer spectra we present in the following are obtained with the values of the neutralizing probability and correction factors for an infinitely thick target.

Power Distribution in the Injected Neutral Beam

The species distribution s characterizes the conditions in the ion source. For the primary purpose of neutral beams, however, it is important to know the power distribution p of the neutral beams heating the plasma. For example, the penetration depth of neutral atoms in a plasma depends very critically on the energy of the atoms. The power distribution is defined by the fractions of the total power carried by neutral hydrogen or deuterium atoms with the different energies. Hence,

$$p_i = P_{E_0/i}/P_{\mathrm{tot}}, \quad i = 1..3, \tag{14}$$

P_{tot} being the total injected power. Here, i denotes neutral hydrogen atoms with an energy of E_0/i, originating from the respective extracted ions by neutralization and dissociation in the case of the molecular ions.

The power $P_{E_0/i}$ carried by neutral atoms with energy E_0/i after neutralizing the extracted ions is given by

$$P_{E_0/i} = A\, j_i^0\, E_0/i \tag{15}$$

A being the total beam area and j_i^0 the neutral atom 'current' density with energy E_0/i. (This equation is only valid if the density profile across the beam is constant, see the assumptions in this section above.) j_i^0 is a certain fraction of the extracted current density of the respective extracted ions; hence

$$j_i^0 = F_{0,i}^{\infty}\, i\, j_i^{\mathrm{ext}}, \tag{16}$$

$F_{0,i}^{\infty}$ being the neutralizing probability for an hydrogen ion with energy E_0/i. The i factor in Eq. 16 origins from the fact, that the H_2^+ and H_3^+ ions dissociate in 2 and 3 neutral H atoms, respectively. Furthermore, j_i^{ext} is a certain fraction of the total extracted current, given by the species distribution Eq. 6. Hence,

$$j_i^0 = F_{0,i}^{\infty}\, i\, s_i\, j_{\mathrm{tot}}^{\mathrm{ext}}. \tag{17}$$

With

$$P_{\mathrm{tot}} = \sum_{k=1}^{3} P_{E_0/i}, \tag{18}$$

the power distribution p_i is then given by

$$p_i = \frac{A\, F^{\infty}_{0,i}\; i\; s_i\; j^{\mathrm{ext}}_{\mathrm{tot}}\; E_0/i}{\sum_{k=1}^{3} A\, F^{\infty}_{0,k}\; k\; s_k\; j^{\mathrm{ext}}_{\mathrm{tot}}\; E_0/k} \qquad (19)$$

Hence, the power distribution can be finally 'extrapolated' from the species distribution in the ion source by weighing the species distribution with the neutralizing probability of each species:

$$p_i = \frac{F^{\infty}_{0,i}\; s_i}{\sum_{k=1}^{3} F^{\infty}_{0,k}\; s_k}, \quad i = 1..3. \qquad (20)$$

3.3.2 Duct Measurements

Power Distribution

After leaving the neutralizer and the magnet, only neutral H^0 or D^0 atoms with the three different energies are left. Hence, H_α/D_α light origins only from collisions of fast neutral atoms with the residual H_2 or D_2 gas in the duct between the beam line and the torus vessel. Hence, the interpretation of the H_α peak intensities of the duct spectra is much simpler than that of the neutralizer spectra.

According to Eq. (5), the Doppler shifted H_α/D_α intensity $I^{\mathrm{d}}_{E_0/i}$ in the duct at E_0/i is then given by

$$I^{\mathrm{d}}_{E_0/i} = B_d\, \sigma_0\, v_i\, n^0_{E_0/i}\, n_{\mathrm{d}}, \qquad (21)$$

Here, B_d is a constant, $n^0_{E_0/i}$ the neutral atom density with energy E_0/i, v_i is the respective velocity of these atoms, n_{d} is the H_2 density in the duct — which is two orders of magnitude lower than in the neutralizer — and σ_0 the excitation cross section by collisions. Figure 5 shows the dependence of σ_0 on the energy per nucleon [18].

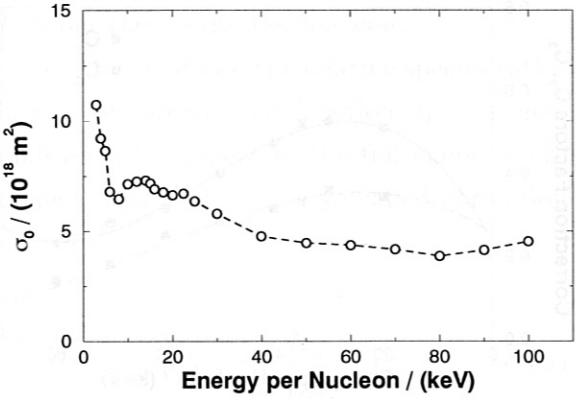

Figure 5: *Excitation cross section σ_0 for collisions of neutral atoms with thermal H_2 gas vs. energy per nucleon [18].*

The assumptions made in Section 3.3.1 for the derivation of Eq. (5) are much better fulfilled in the duct than in the neutralizer. Especially, the hydrogen background pressure in the duct is so low, that the species distribution is not changed in the region between the exit of the neutralizers and the duct. Hence, all effects concerning a non-uniform H_2 pressure profile — e.g. different conditions in the exciting and viewing regions — can be neglected.

As above, the power carried by the neutral atoms with energy E_0/i is given by

$$P_{E_0/i} = A\, j^0_i\, E_0/i. \qquad (22)$$

The neutral beam 'current' density

$$j^0_i = n^0_{E_0/i}\, v_i \qquad (23)$$

can be expressed as

$$j^0_i = \frac{I^{\mathrm{d}}_{E_0/i}}{\sigma_0\, n_{\mathrm{d}}}. \qquad (24)$$

Hence, the power distribution p^{d}_i, obtained from the H_α measurements in the duct, is given by

$$p^{\mathrm{d}}_i = \frac{I^{\mathrm{d}}_{E_0/i}}{i\,\sigma_0} \Bigg/ \sum_{k=1}^{3} \left(\frac{I^{\mathrm{d}}_{E_0/k}}{k\,\sigma_0} \right). \qquad (25)$$

If the assumptions of the applicability of the models for the generation of neutral atoms from the extracted ion species and the emission of H_α light and the different cross sections are correct, the power distribution, derived from the duct measurement in Eq. (25), should be equal to the power distribution, derived from the neutralizer measurements in Eq. (20).

3.4 Gaussian Fit to Spectra

The spectra are fitted after subtraction of the main H_α/D_α peak by a sum of three Gaussians (one Gaussian per peak) with a third order polynomial background:

$$y_{\text{fit}} = y_{\text{b}} + \sum_{j=1}^{3} g_j \tag{26}$$

with

$$g_j = g_{0,j} \exp\left(-\frac{(\lambda - \lambda_{0,j})^2}{2\,\Delta\lambda_j^2}\right), \quad j = 1..3, \tag{27}$$

and

$$y_{\text{b}} = \sum_{k=0}^{3} b_k \lambda^k, \tag{28}$$

λ being the wavelength, and j denoting the three different peaks.

The 13 fit parameters ($g_{0,j}, \lambda_{0,j}, \Delta\lambda_j$ for $j = 1..3$ and the b_k's) are obtained by a least square fit to a non-linear function by minimizing

$$\chi^2 = \sum_{k=1}^{N} \left(\frac{(y_k - y_{\text{fit}}(\lambda_k))^2}{y_k}\right) \tag{29}$$

the y_k's being the experimental data points, $y_{\text{fit}}(\lambda_k)$ the fitting value at the position λ_k of the data point y_k, and N the number of data points (usually 800 to 1000).

Neutralizer Spectra

Figure 6(a) shows the results of the fitting routine for the spectrum shown in Figure 2(a) measured in the neutralizer of source NW3 for a 60 kV deuterium beam. The fit parameters of the Gaussians as well as the parameters necessary for the calculation of the species and power distributions are also given in the figure. The fitted spectrum matches the measured spectrum rather well, with the exception of the left wing of the Doppler shifted peaks. This left wing corresponding to lower energies was also observed in the JET Neutral Beam Testbed spectra and may be caused by ions which have not been accelerated to the full energy [19]. These ions were either neutralized before gaining the full energy or are created inside the acceleration region. In the JET neutral beam testbed, this fraction of not fully accelerated ions is up to 10% for the full energy and up to 30% for the half energy particles, respectively, depending on the gas flow into the neutralizer.

The small mismatch of the peak maximum between fit and measured spectrum in Figure 6(a) may indicate a two-Gaussian structure in the single peaks; however, the mismatch is too small to draw firm conclusions. If indeed the not-fully accelerated ions cause the peak shape deviations from Gaussians, the amount of these ions in the ASDEX Upgrade beamlines are of the same order of magnitude as in the JET testbed; but there are other mechanism which can influence the peak shape, such as angle asymmetries of the single beamlets.

In the above spectrum, the fitted peak positions are blue shifted with respect to the experimental peak positions by about 0.04 nm

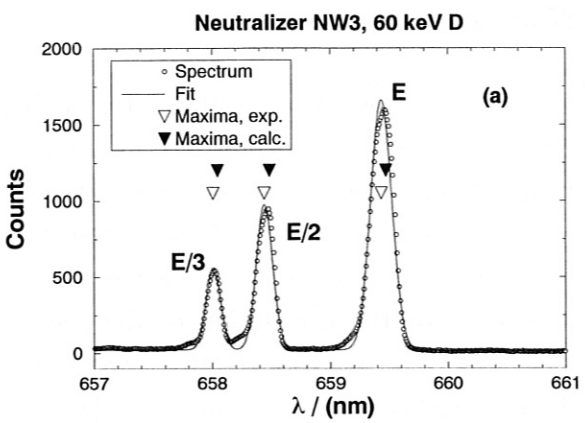

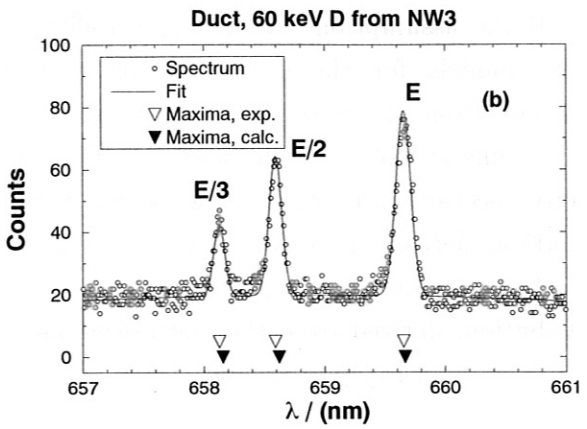

	$i=3$	$i=2$	$i=1$	
$g_{0,i}$	548	963	1630	
$\triangle\lambda_i$	0.060	0.068	0.089	nm
$\lambda_{0,i}$	658.01	658.44	659.43	nm
$\lambda_{0,i}^{calc}$	658.05	658.48	659.47	nm
$I_{E_0/i}$	13.4	26.7	59.9	%
C_i	0.23	0.32	1.0	
$F_{0,i}^{\infty}$	0.81	0.72	0.44	
s_i	4.3	12.0	83.7	%
p_i	7.1	17.6	75.3	%

	$i=3$	$i=2$	$i=1$	
$g_{0,i}$	22.7	44.5	59.3	
$\triangle\lambda_i$	0.047	0.053	0.062	nm
$\lambda_{0,i}$	658.13	658.59	659.65	nm
$\lambda_{0,i}^{calc}$	658.16	658.62	659.67	nm
$I_{E_0/i}$	15.0	33.1	51.9	%
$\sigma_{0,i}$	7.08	7.21	5.86	10^{14} m^2
p_i	5.9	19.3	74.7	%

Figure 6: *Fit to the D_α spectra shown in Fig. 2, measured in (a) the neutralizer of source NW3 and (b) in the duct of the NW beamline. The fit parameters of the Gaussians (see Eq. 27), theoretical peak positions λ_0^{calc}, peak integrals I, correction factors C, asymptotic neutral beam fraction F_0^{∞}, excitation cross section σ_0, and species s and power p distributions, respectively, are shown in the lower tables.*

for all peaks. This may reflect the above mentioned small deviations of the peaks from a Gaussian structure. However, this mismatch between calculated and experimental peak positions depends on the ion source. Hence, it is caused most probably by a misalignment of the viewing angle of some tenths of degrees — about 0.5° in the example above.

A similar fit to the H_α spectrum with a sum of three Lorentzian curves, as suggested by Kamperschroer for his TFTR spectra [13], results in a rather bad matching. Furthermore, we do not have to assume complex background functions with steps as well as a second broad Gaussian for each peak, as it was the case for the W7-AS beams [12].

Duct Spectra

Figure 6(b) shows the result of the fitting routine to the duct spectrum shown in Figure 2(b). The peaks can be well described by Gaussian functions. The fit parameters of the

Gaussians as well as the parameters necessary for the calculation of the power distribution are also given in the figure.

Due to the smaller signals and thus the higher signal-to-noise ratio, the deviations of the single Gaussian fits from the measured peaks are not so pronounced as for the neutralizer spectrum. Again, the peaks are blue shifted with respect to the calculated peak positions by about 0.03 nm, again indicating a misalignment of the viewing angle of about 0.4 degree in this case.

3.5 Errors

The calculated species and power distributions are as 'good' as the models, describing the evolution of the species from the source to the neutralizer, and the input parameters used in the calculations. The main parameters, which influences the species distribution, are the correction factors C_i. A comparison by Bilau-Faust [9] of these factors calculated by different authors (and models) showed that the maximum difference in the C_i's was about 10%. This leads to an error of about $\pm(1-2)$ percentage points in the full energy component.

As already mentioned in the discussions above, the density profile of the neutralizer gas from the ion source to the viewing point in the neutralizers is the most crucial point. For simplicity and due to the limited knowledge, we assumed in the discussions of the neutralizer measurements above, that the pressure profile is constant from the ion source to the viewing region and that the target thickness is large enough so that there is no change of the species distribution from the region of creating the excited ions and the viewing region.

A calculation with corrections factors for a finite target thickness of 2×10^{19} m^{-2} — instead of the 'infinite' value of 2×10^{20} m^{-2} — resulted in a full energy component fraction of the power distribution of about 5 percentage points lower (about 60% for the arc sources and 60 kV deuterium instead of 65%); the fractions of the other components were accordingly larger by about 2.5 percentage points. However, this target thickness is certainly too low; hence, the overall error of the species and power distributions may be about ±3 percentage points for the full energy component for the neutralizer spectra. The error of the power distribution obtained from the duct spectra is somewhat lower, due to the much simpler interpretation of these spectra.

4 Results

4.1 Neutralizer Measurements of Deuterium Beams

4.1.1 RF Source

Figure 7 shows the dependence of the species and power distributions of the RF sources on the RF input power P_{RF}. In order to minimize the electron current to the back plate of the ion sources, the gas flow into the ion sources for the low RF power beams are reduced by about 35%. Accordingly, the gas flow in the neutralizers are also reduced.

Both distributions show similar trends. The fraction of the full energy component (D^+ or $D^0(E)$, respectively) increases with increasing RF input power, whereas the fraction of the third energy components (D_3^+ or $D^0(E/3)$, respectively) decreases with increasing RF input power. The fraction of the half energy components remains practically unchanged. It can also be seen in the figure,

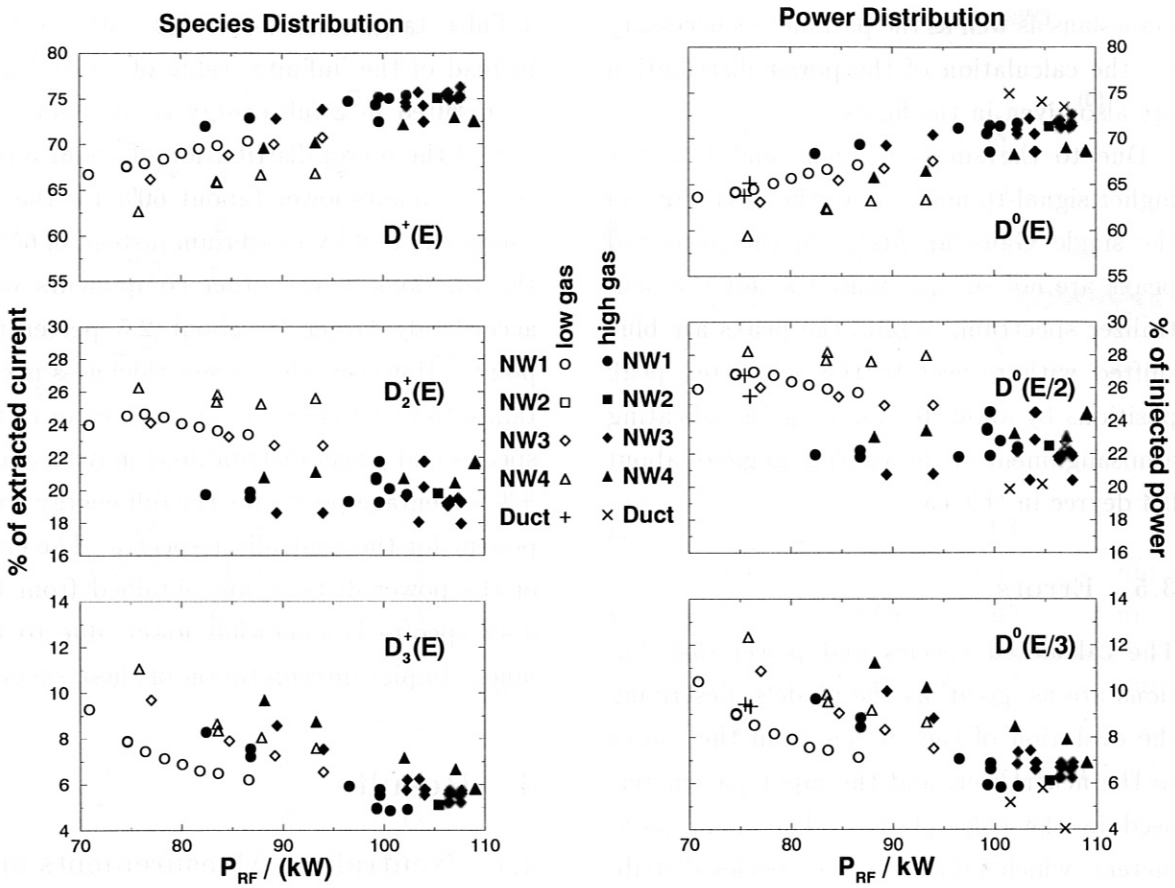

Figure 7: *Species and power distribution vs. RF input power for three of the four sources of the NW ASDEX Upgrade beam line for deuterium beams. 'low gas' refers to gas flows of about 16 mbar l/s in the ion source and about 50 mbar l/s in the neutralizer; 'high gas' refers to gas flows of about 22 mbar l/s in the ion source and about 60 mbar l/s in the neutralizer, respectively.*

that both distributions depend also on the gas input flow in the ion source; the fact that the power distribution shows the same dependency on P_{RF} as the species distribution indicates, that the gas flow into the neutralizers does not affect the power distribution. This indicates again, that the target thickness of the neutralizers is large enough, so that the neutralizing probability does not depend on this quantity (see Eq. 9).

The fraction of D^+ ions increases with increasing gas flow into the ion source. This can be explained by the increasing cracking probability of the deuterium molecular ions: the more gas in the source, the more collisions take place.

The species and power distributions depend also on the special conditions in the ion sources. This can be seen also in Figure 7, where the source NW4 delivers less full energy atoms than the other three sources. The reasons for the source discrepancies are not clear; perhaps it can be related to the coupling of the RF power to the plasma: again the source NW4 shows a higher divergence of the beamlets at the perveance optimum. Both the species distribution and the divergence are influenced by the electron density

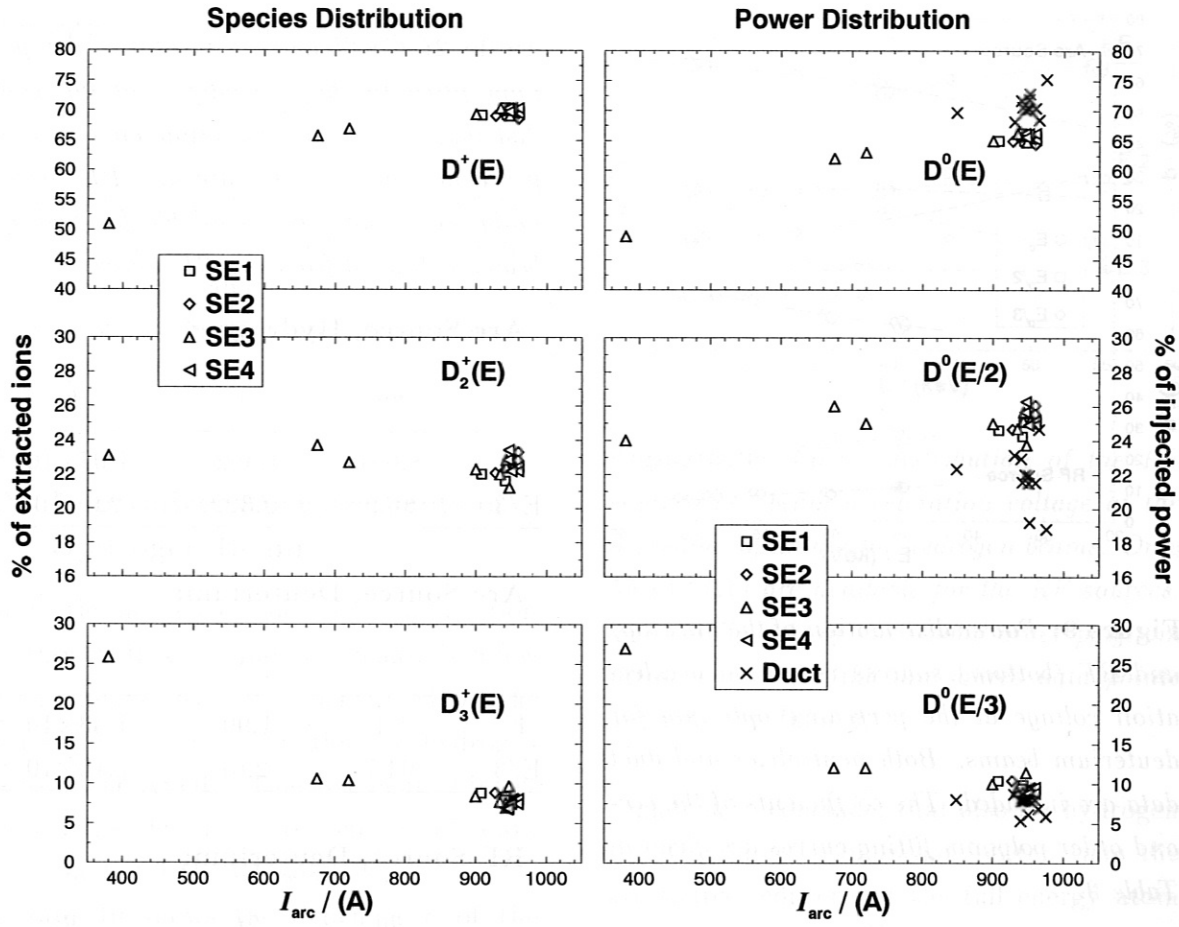

Figure 8: *Species and power distribution vs. arc input power for 60 kV deuterium beams, measured in the duct and in the neutralizers of the arc sources SE1 to SE4 of the SE ASDEX Upgrade beamline.*

and temperature profiles in the ion source and hence by the RF coupling. Furthermore, this source needs more RF power for the same extraction current, compared with the other three sources [20].

The data in Figure 7 were obtained by changing the RF input power at steps of the acceleration voltage of 45 kV, 50 kV, 55 kV and 60 kV, hence changing also the perveance of the beams. As can be seen in the figure, this perveance scan does not influence the slope of the curves. This indicates, that the species and power distributions of the ASDEX Upgrade RF sources do primarily depend on the RF input power and the gas flow into the ion source, and not on the extraction voltage, as it can be expected.

4.1.2 Arc Source

Figure 8 shows the dependence of the species and power distributions of the ASDEX Upgrade arc sources on the arc current applied to the ion sources. The data base is rather limited, due to the lack of experimental time; the beam line was mostly run at the 'design' values (60 kV at the perveance optimum) for injection.

As it was also shown for the RF sources,

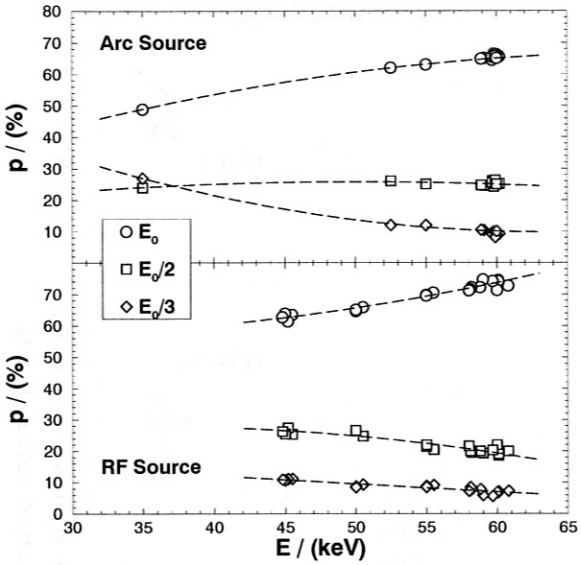

Figure 9: *Power distribution of the arc (top) and RF (bottom) sources vs. beam acceleration voltage at the perveance optimum for deuterium beams. Both neutralizer and duct data are included. The coefficients of the second order polynom fitting curves are given in Table 2.*

the fraction of the full energy component increases with increasing input power, in this case with increasing arc current. Furthermore, all four sources of the SE beam line behave rather similarly.

4.1.3 Power Distribution vs. Extraction Voltage

Although the species and power distributions of the neutral beams depends primarily on the input power at the ion source (i.e. the arc current and the RF power, respectively), it is convenient to express the species and power distribution as a function of the beam energy. This is due to the fact, that the beam energy (and the power) is the important parameter for the plasma. On the other hand, if the beams are run at the perveance optimum, the source input power is a monotonically increasing function of the beam acceleration voltage.

Table 2: *Coefficients of the two order polynom fitted to the dependence of the power distribution on the extraction energy at the perveance optimum for arc and RF sources. Only 55 kV data are available for hydrogen beams extracted from the RF sources.*

Arc Source, Hydrogen:

	a_0	a_1	a_2
E	8.691	1.362	-1.07×10^{-2}
E/3	86.0	-2.322	2.0×10^{-2}

Arc Source, Deuterium:

	a_0	a_1	a_2
E	-1.18	1.90	-1.33×10^{-2}
E/3	94.7	-2.67	2.10×10^{-2}

RF Source, Deuterium:

	a_0	a_1	a_2
E	64.2	-0.62	1.29×10^{-2}
E/3	23.5	-0.30	4.10×10^{-4}

Figure 9 shows the dependence of the power distribution of deuterium beams on the beam energy for the arc and RF sources of ASDEX Upgrade. Data are only taken at the perveance optimum. Both neutralizer and duct data are included. With increasing beam energy, the proton content also increases. This reflects the higher input power into the source. The dependence of the amounts of the E_0 and the $E_0/3$ species component are

fitted with a second order polynom:

$$p_i^f = \sum_{k=0}^{2} a_k \, U_{ex}^k[\mathrm{kV}], \qquad (30)$$

the respective function for the half energy component can be obtained by subtracting the E_0 and $E_0/3$ values from unity. The parameters of the fits to the deuterium beams for the arc and RF sources are given in Table 2.

4.2 Neutralizer Measurements of Hydrogen Beams

Due to the limited use of hydrogen injection into the ASDEX Upgrade plasma, only a few measurements have been performed on the species and power distributions of hydrogen beams of the ASDEX Upgrade neutral injection sources. Furthermore, only 55 kV data are available for the RF sources.

Figure 10 shows the dependence of the power distributions of the arc and RF sources on the extracted energy at the perveance optimum for hydrogen beams. Due to the dependence of the optimum beam current on $U_{\mathrm{ex}}^{3/2}$, the curves also reflects the dependence of the power distribution on the source input power (for the arc sources). The mean values for the power distributions of 55 kV hydrogen beams extracted from both types of ion sources are listed in Table 3.

As in the case for deuterium beams (see also Section 5.1), the RF sources deliver a higher fraction of the full energy component and accordingly a lower fraction of the third energy component. The half energy fraction remains rather unchanged. However, the respective values are just within the error bars. But due to the similarity of the trends for both hydrogen and deuterium beams, we feel

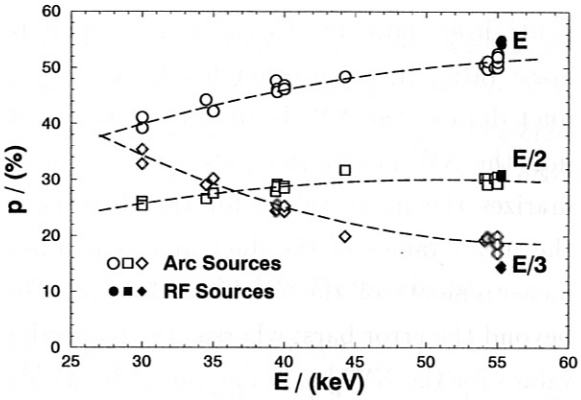

Figure 10: *Power distribution of the RF sources vs. beam acceleration voltage at the perveance optimum for hydrogen beams. Only 55 kV data are available for the RF sources. The coefficients of the second order polynom fitting curves for the arc source data points are given in Table 2.*

confident to conclude, that also for hydrogen the RF source is somewhat 'better' than the arc source, concerning the full energy atom yield.

4.3 Duct Measurements of Deuterium Beams

Measurements of the power distribution for 60 kV deuterium beams have been performed for both beam lines in the neutral beam injection duct of ASDEX Upgrade during shots into the 'empty' torus (see above); furthermore, in the case of the NW beamline, data also for 45 kV deuterium beams are available.

The resulting power distributions are also included in Figures 7 and 8. Due to the MSE gauging procedures (see Section 5.2), there are much more data points for the SE beam line. There is a trend of an increased full energy fraction of the neutral beams, especially for the SE beam line. The duct data, however, show a much larger scatter than the

neutralizer data due to the larger signal to noise ratio. On the other hand, the 45 kV duct data of the NW beam line fit very well into the NW neutralizer data. Table 4 summarizes the mean values for the three case; the mean values of the duct and neutralizer measurements of the SE beam line may be beyond the error bars; whereas the respective values for the NW beam line might be within the error bars.

5 Discussion

5.1 Comparison RF - Arc Source

The resulting mean values for the species and power distributions for the RF and arc sources for a 60 kV deuterium beam are summarized in Table 4. The full energy fraction of the injected neutral beam is higher for the RF sources (about 72% compared to about 65% for the arc sources). This difference is clearly well outside the error bars. Accordingly, the amounts of deuterium molecular ions extracted from the RF sources are reduced.

The reason for the 'better' behavior of the arc source is not quite clear. As was shown in Section 4.1.1 for the RF sources, the fraction of the full energy species increases with increasing gas flow into and thus a higher pressure in the ion source. However, the arc sources have been operated at higher gas flow. Hence, differences in the gas pressure in the respective sources cannot explain the higher proton fraction of the RF sources.

Of course, the different plasma generating methods lead to different electron temperature and density profiles in the ion source which influences the species distribution. Typical mean electron energies in RF sources are of the order of 10 eV [22], whereas the electrons in an arc source have energies of the order of 100 eV. Furthermore, the cross section for the dissociation of an H_2 molecule by electron collisions has a maximum at about 15 eV to 20 eV [23]. Hence, the degree of dissociation — and therefore the proton fraction — is much higher in an RF source compared to an arc source. (This expected higher proton fraction was also a reason for the development of the RF sources.) However, due to the lack of experimental data, a correlation between electron temperature and density profiles and the species distribution in the ion source can not be made up to now.

Table 3: *Power distributions of the arc and RF sources for a 55 kV hydrogen beam.*

Source	E_0	$E_0/2$	$E_0/3$	
Arc	52.2	30.1	18.7	%
RF	54.6	30.9	14.5	%

The influence of the magnetic field configuration — and hence the electron density and temperature profiles — on the species distribution can be seen in the fact that the JET arc sources deliver a much higher proton fraction than the ASDEX Upgrade arc sources. Typical values are 86% D^+ ions for a 72 kV deuterium beam [19], with 10% and 4% D_2^+ and D_3^+ ions, respectively. The JET sources are equipped with a so-called super-cusp configuration, with magnetic field lines reaching through the source plasma [24] (this configuration has, however, the drawback of a higher non-uniformity of the current profile across the beam). In contrast, the chequerboard configuration of the magnets of the ASDEX Upgrade sources leads to magnetic fields only

Table 4: *Comparison of the power distributions of the ASDEX Upgrade neutral beam lines (arc and RF sources) measured in the neutralizer and in the duct. The RF data are without the NW4 data. Also included are the results of the MSE diagnostic measurements in the torus. The error is about ±3 percentage points in the full energy component for the neutralizer data and about ±2 percentage points for the duct data.*

Arc sources, 60 kV Deuterium:

Location	E_0	$E_0/2$	$E_0/3$	
Neutralizer:				
this work	65.5	25.1	9.3	%
Ref. [21]	65.1	24.8	10.1	%
Duct:				
mean	70.6	21.9	7.5	%
#10751	68.2	23.1	8.7	%
Torus (MSE):				
mean	67.3	24.2	8.5	%
#10751	68.3	23.7	8.0	%

RF sources, 60 kV Deuterium:

Location	E_0	$E_0/2$	$E_0/3$	
Neutralizer	71.6	21.9	6.5	%
Duct	74.2	20.8	5.0	%

RF sources, 45 kV Deuterium:

Location	E_0	$E_0/2$	$E_0/3$	
Neutralizer	63.4	25.9	10.7	%
Duct	64.5	26.1	9.4	%

in the vicinity of the chamber walls (which has the advantage of a more uniform beam).

Apart from the electron 'configuration' in the ion source, the source wall material also influences the species distribution. First measurements of the species distribution of the ASDEX Upgrade RF prototype source revealed a proton fraction of about 80% for a 45 kV deuterium beam [9, 25]. This source was equipped with a quartz wall, which is necessary to protect the RF coil from the plasma. Furthermore, the coating of a fraction of the copper backplate of the source with aluminum oxide in order to reduce the hydrogen recombination at the chamber walls increased the proton fraction further by about five percentage points [25].

However, wall effects cannot explain the proton enhancement of the ASDEX Upgrade RF sources with respect to the arc sources. Due to the contact with the source plasma, the quartz wall of the prototype source was damaged by erosion. Therefore, a Faraday screen made out of copper was inserted between the quartz vessel and the plasma. Hence, both source types at ASDEX Upgrade have metal walls with similar hydrogen recycling properties.

5.2 Comparison Neutralizer - Duct Measurements

In spite of the fact, that there might be a trend to a higher full energy component fraction in the duct measurements, the agreement of the power distribution obtained from the duct spectra with that from the neutralizer spectra is rather good taking into account the simplified assumptions on the gas density profile and the target thickness in the neutralizer data evaluation. The duct values in Table 4 are mean values; however, as can be seen in Figure 6, the duct and neutralizer values for

single shots may be closer together, reflecting the limited data base. The better match of the 45 kV values — where the target thickness necessary for infinitely thick target conditions is lower — may indicate that the larger disagreement at the higher energies can be due an increasing (small) deviation of the target thickness from the assumed infinitely target conditions.

The rather good agreement of the power distributions obtained from the neutralizer and duct spectra demonstrates also the good uniformity of the beams: due to the different viewing geometries in the neutralizer (from top) and in the duct (from the side), different parts of the beams are averaged in an H_α spectrum (see Section 3.1).

In order to measure locally the radial electric field strength in the ASDEX Upgrade plasma, a MSE (Motional Stark Effect) diagnostic was recently installed at ASDEX Upgrade [26]. This diagnostic measures the Stark splitting of the Doppler-shifted full energy line during neutral injection in the plasma at 10 different points of the neutral path through the plasma. The MSE diagnostic is 'fixed' to the source SE3. Normally, only a small wavelength range (about 2 nm) around the full energy peak is monitored. However, in order to gauge the position of the line, also full range spectra has been measured during the the installation of this diagnostic. This was done during the same experiments mentioned above, where a neutral beam was injected into the 'empty' torus.

During the MSE gauging procedure, only three full range spectra suitable for our analysis have been monitored. Unfortunately, only one of the injection shots (#10751) was monitored simultaneously by the MSE diagnostic and by our duct system due to trigger problems. Table 4 summarizes both the mean power distributions derived from our duct and from the MSE measurements as well as the power distribution for the shot #10751. Whereas our duct mean value is somewhat higher than the MSE mean value, the power distributions of both measurements for shot #10751 are quite similar. This reflects the small database of the MSE spectra. However, we can conclude, that both measurements of the power distribution are consistent: the power distribution that have been measured in the duct is also injected into the plasma.

Table 5: *Estimated power distribution of deuterium beams for the 100 kV RF sources (see text).*

D^0	E_0	$E_0/2$	$E_0/3$	
p_i	60	26	14	%

5.3 Extrapolation to the 100 kV Deuterium RF Sources

The obtained fit formulas cannot be extrapolated to the new 100 kV sources of ASDEX Upgrade in the NW beam line (start of operation: Dec. 1998); these sources will be run at lower extracted currents (60 A instead of about 80 A) in order to inject the same input power as the 60 kV sources into the plasma. Hence, the input RF power into the plasma source will also be reduced. Table 5 shows the power distribution for 100 kV deuterium beams, estimated from the RF power (about 70 kW), which is necessary for the extraction of about 60 A per source; see Figure 7.

6 Summary

The species and the power distributions of the ASDEX Upgrade neutral beam lines have been measured by H_α Doppler shift spectroscopy. The results can be summarized as following:

- The newly installed RF sources yield higher full energy neutrals than the arc sources.
- The amount of full energy neutral atoms in the RF sources rises with increasing RF input power and gas flow in the ion source.
- Similarly, the amount of full energy neutral atoms in the arc source rises with increasing arc current applied to the source.
- The measurements of the power distribution in the duct reveal a slightly higher amount of full energy power than the extrapolation of the neutralizer measurements; they are consistent with power distributions derived from MSE spectra in the torus.

The mechanism leading to the higher full energy fraction yield of the RF sources with respect to the arc sources may be caused by the higher degree of dissociation in the RF sources due to typical electron temperatures near the maximum of the cross section of the dissociation of hydrogen molecules; detailed measurements of the electron temperature and energy distributions in the respective ion sources are necessary for a better understanding. The slightly higher power distributions measured in the duct indicate that there might be some (small) corrections of the assumptions in the models describing the evolution of a extracted particle from the source through the neutralizer and the duct into the torus are necessary.

7 Appendix: Example of Data Sheet

Figure 7 shows as an example the computer generated data sheet with the beam data, the results of the fitting routines, the fit parameters, and the calculated species and power distributions. The symbols and text inserts have following meanings:

- The first three lines in the plot insert list the experimental settings: the spectrum was measured in source 3 of the NW beam line for a deuterium beam with 60.1 kV extraction voltage and 107.7 kW RF input power; this leads to beam current of 83.3 A and a perveance of 5.66×10^{-6} A/V$^{3/2}$.
- The experimental spectrum is drawn by the solid line, the fitted one by the dashed line.
- The solid diamonds at the Doppler shifted peaks denote the theoretical position of the peaks, the open diamonds the fitted peak positions.
- The species and power ('Leistung') distributions are given by the numerical integration of the peaks ('Spektr.') with the integration limits denoted by the open circles and by the integration of the fitted Gaussians ('Fit'). In this case, both methods reveal almost identical values.

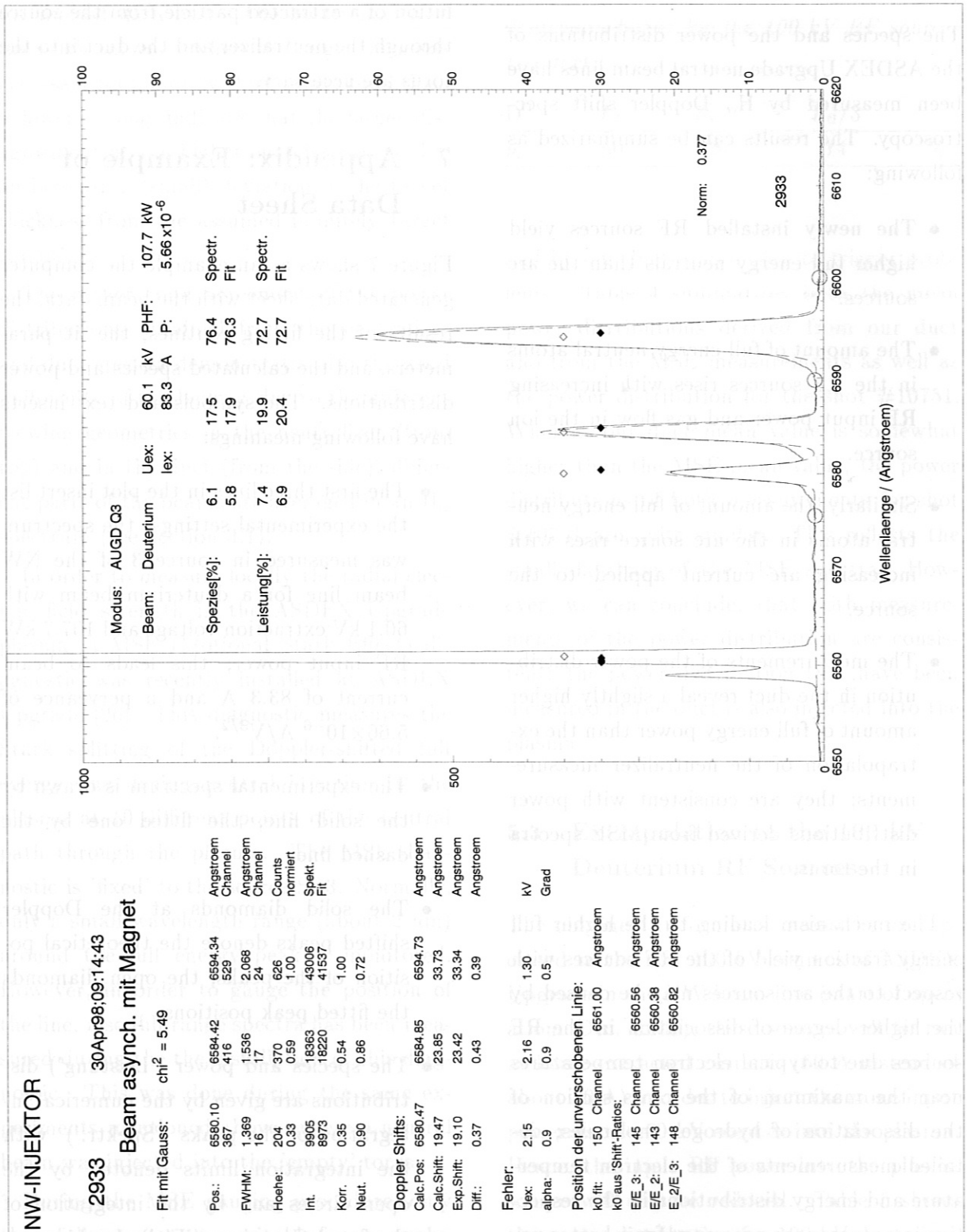

Figure 11: *Example of a data sheet generated by the H_α fitting routine*

- The first three lines on the left side of the data sheet list the beam line (NW), shot number, date and time, and the mode of operation.
- The next lines give the quality of the fit ('chi^2') and the fit parameters for each peak: position ('Pos.'), FWHM — both in Å and channels — and height ('Hoehe') for the $E_0/3$, $E_0/2$ and E_0 component.
- The next lines list the parameters necessary for the calculation of the species and power distributions: the peak integrals (numerically and by the fitted Gaussians), the correction factors ('Korr.') and the neutralizing probability ('Neut.')
- The next lines show the differences between the calculated Doppler shifts and the fitted values; they can be explained by errors ('Fehler') in U_{ex} or in the viewing angle α
- Finally, the position of the unshifted line, λ_0, is cross-checked by the positions the Doppler shifted lines, λ_i, by

$$\lambda_0 = \frac{\lambda_i - \sqrt{j/i}\,\lambda_j}{1 - \sqrt{j/i}}, \quad i,j = 1..3, i \neq j. \tag{31}$$

The solid diamonds at the unshifted D_α line show the cross checked positions.

Acknowledgements

The authors would like to thank Robert Wolf for making available the MSE data.

References

[1] E. Speth. Rep. Prog. Phys. **52** (1989) 57.

[2] C.F. Burrel, W.S Cooper, W.F. Steele, and R.R. Smith. Calorimetric and optical beam diagnostics in the LBL 120 keV neutral beam test facility. In *Proceedings of the 7th Symposium on Engineering Problems of Fusion Research, Knoxville, Tennessee, USA* (1977), vol. 1, p. 374.

[3] C.F. Burrel, W.S. Cooper, R.R. Smith, and W.F. Steele. Rev. Sci. Instrum. **51(11)** (1980) 1451.

[4] O. Vollmer, A. Stäbler, J.H. Feist, K. Freudenberger, B. Heinemann, H. Lohnert, S. Obermayer, R. Riedl, W. Schärich, E. Speth, and K. Wittenbecher. Commissioning and first operation of the ASDEX Upgrade neutral beam system. In *Proceedings of the 15th IEEE/NPSS Symposium on Fusion Engineering* (Hyannis, MA, 1993).

[5] G. Düsing, H. Altmann, H. Falter, A. Goede, R. Haange, R.S. Hemsworth, P. Kupschus, D. Stork, and E. Thompson. Fusion Technology **11** (1987) 163.

[6] A. Stäbler, F. Ryter, P. Franzen, O. Gruber, S. Günther, M. Maraschek, V. Mertens, O. Vollmer, and The ASDEX Upgrade Team. Operational window and performance at high heating power in the ASDEX Upgrade tokamak. In *Proceedings of the 20th Symposion on Fusion Technology, Marseille, France* (1998), Association EURATOM - C.E.A., Cadarache.

[7] W. Kraus, J.H. Feist, and E. Speth. Optimization of a large area RF plasma generator. In *Proceedings of the 19th Symposium on Fusion Technology* (Lisboa, Portugal, 1996), p. 649.

[8] O. Vollmer, A. Stäbler, E. Speth, M. Ciric, P. Franzen, B. Heinemann, W. Kraus, W. Melkus, R. Riedl, and W. Schärich. Commissioning and performance of the new ASDEX Upgrade neutral beam injector. In *Proceedings of the 20th Symposion on Fusion Technology, Marseille, France* (1998), Association EURATOM - C.E.A., Cadarache.

[9] R. Bilau Faust. Spektrometrische Messung der Speziesverteilung sowie der Strahldivergenz von Wasserstoff- und Deuteriumstrahlen der Ionenquellen der ASDEX NI-Beamline sowie der HF-Quelle. Tech. Rep. IPP 4/245, Max-Planck-Institut für Plasmaphysik, Garching, Germany, 1991.

[10] G. Bracco, C. Breton, C. De Michelis, M. Mattioli, and J. Ramette. Balmer-series emission cross-sections for the interaction between hydrogen neutral beams and molecular hydrogen: an annotated bibliography. Tech. Rep. EUR-CEA-FC-1040, Association EURATOM - C.E.A., Fontenay-aux-Roses, France, 1980.

[11] J. Kim and H.H. Haselton. J. Appl. Phys. **50(6)** (1979) 3802.

[12] W. Ott and F.P. Penningsfeld. Spectroscopic determination of species and divergence of hydrogen beams in the W7AS neutral beam injectors. Tech. Rep. IPP 4/258, Max-Planck-Institut für Plasmaphysik, Garching, Germany, 1993.

[13] J.H. Kamperschroer, L.R. Grisham, N. Kokatnur, L.J. Lagin, R.A. Newman, T.E. O'Connor, T.N. Stevenson, and A. von Halle. Doppler shifted neutral beam line shape and beam transmission. Tech. Rep. PPPL-2981, Princeton Plasma Physics Laboratory, 1994.

[14] W. Ott. Private communication.

[15] S.K. Allison. Reviews of Modern Physics **30**, 4 (1958) 1137.

[16] R.S. Hemsworth. Species determination using Doppler shift spectroscopy for non-equilibrium hydrogen ions and/or neutral beams. Tech. Rep. JET-DN-C(85)8, JET Joint Undertaking, 1985.

[17] J. Pamela. Rev. Sci. Instrum. **57** (1986) 1066.

[18] I.D. Williams, J. Geddes, and H.B. Gillbody. J. Phys. B **15** (1982) 1377.

[19] D. Ciric, H.-D. Falter, and D.J. Godden. Space and time resolved Doppler spectroscopy of neutral beams. In *Proceedings of the 20th Symposium on Fusion Technology, Marseille, France* (1998), vol. 1, p. 469.

[20] P. Franzen. Unpublished results.

[21] O. Vollmer. Unpublished results.

[22] W. Kraus. Massenspektrometer für strahldiagnostische Messungen an der Hochfrequenzionenquelle RIG 10 und Untersuchungen im Hinblick auf hohe Protonenströme und Reinheit des Strahls. Master's thesis, Justus-Liebig-Universität Gießen, 1981.

[23] S. Chung, C.C. Lin, and E.T.P. Lee. Phys. Rev. A **12(4)** (1975) 1340.

[24] D.J. Godden. PINI ion source uniformity and the magnetic field structure. In *Proceedings of the JDC Meeting 1/96, JET* (21-22 May 1996).

[25] W. Kraus, J.H. Feist, E. Speth, and M. Lochter. A high power RF plasma source for neutral beam injection systems. In *2nd German-Russian Conf. on Electric Propulsion Engines and Their Technical Applictaions, Moscow, Russia* (1993).

[26] R. C. Wolf, P. J. McCarthy, F. Mast, H.-P. Zehrfeld, and ASDEX Upgrade Team. Motional stark effect polarimetry for the determination of the ASDEX Upgrade current density profile. In *Europhysics Conference Abstracts (Proc. of the 24th EPS Conference on Controlled Fusion and Plasma Physics, Berchtesgaden, 1997)* (Petit-Lancy, 1997), M. Schittenhelm, R. Bartiromo, and F. Wagner, Eds., vol. 21A, part IV, EPS, pp. 1509–1512.